RP Current Trends In Applied Sciences
Vol. 3, No. 4 (October – December 2024) pp. 80–86
e-ISSN: 2583-7486

RESEARCH PLATEAU PUBLISHERS

Cite this article: Ajit Singh, Effects of band nonparabolicity and carrier heating on parametric gain in polar semiconductors, *RP Cur. Tr. Appl. Sci*. **3** (2024) 80–86.

Original Research Article

Effects of band nonparabolicity and carrier heating on parametric gain in polar semiconductors

Ajit Singh*
Assistant Professor, Department of Physics, Government College, Kalka – 133302 (Panchkula) Haryana, India
*Corresponding author, E-mail: ajitnehra2010@gmail.com

ARTICLE HISTORY
Received: 12 July 2024
Revised: 02 Dec. 2024
Accepted: 10 Dec. 2024
Published online: 12 Dec. 2024

KEYWORDS
Polarons and electron–phonon interactions;
Collective excitations;
High-frequency effects.

ABSTRACT
The influence of band nonparabolicity and carrier heating on nonlinear wave dynamics, resulting from parametric interactions between electrons and longitudinal optical phonons in polar semiconductors, has been analyzed both theoretically and numerically. Explicit expressions for the threshold pump necessary to initiate polaron-induced parametric interactions, as well as the corresponding amplification characteristics, have been derived. It is observed that the effects of polarons and band nonparabolicity are cumulative, leading to a substantial increase in parametric gain. At low magnetic fields and moderate carrier concentrations, the energy dependence of the effective electron mass and collision frequency significantly modifies both the threshold and amplification behavior, suggesting potential applications in the design of optical switching devices.

1. Introduction

Polarons have received considerable attention due to their role in forming two-dimensional electron gases in semiconductor heterostructures. The electronic properties of spherical quantum dots under parabolic confinement and dc electric fields [1], as well as the nonlinear optical and quantum characteristics of low-dimensional semiconducting systems [2], have been investigated for potential applications in electronic and photonic devices. Compound semiconductors serve as ideal hosts for studying both 2D and 3D polarons, with InSb being particularly notable for its strongly nonparabolic conduction band [3-7]. Band nonparabolicity significantly influences electronic excitations in doped semiconductors [8]. Earlier studies often treated polaronic effects and nonparabolicity as simply additive; however, incorporating nonparabolicity improves the agreement with experimental observations, including enhanced polaron effective mass renormalization and shifts of resonant polaron behavior to higher fields [9]. Full consideration of nonparabolicity aligns well with experimental results, such as the carrier-concentration dependence of the intensity-vanishing point in infrared reflection spectra [10-12]. Techniques like the Random Phase Approximation combined with Lorentzian oscillator models have been employed to describe phonon polarization [13-15]. Advances in epitaxial growth also make it possible to fabricate Morse quantum wells, where the inclusion of electron–longitudinal optical phonon interactions significantly affects nonlinear optical properties and modifies the optical refractive index [16-18].

Significant changes in polar semiconductors at room temperature and below have been attributed to lattice impact ionization by hot carriers [19-21]. The study of carrier heating (CH) effects in semiconductor plasmas has a long history, dating back to 1973 [8]. In doped semiconductors, strong space-charge fields prevent simple redistribution of carriers, yet nonlinearity can emerge due to the energy dependence of the carrier effective mass. Incorporating appropriate collision mechanisms, Hall field effects, and conduction band nonparabolicity has enabled more realistic analyses of convective instabilities [22]. Carrier heating induced by high-intensity pumps in high-mobility semiconductors has attracted significant research interest, highlighting phenomena such as high transparency, large third-harmonic amplification, and pump attenuation under magnetic fields [23, 24]. Recent studies have also examined the laser induced carrier heating effects on real and imaginary parts of Raman susceptibility of weakly-polar semiconductor magneto-plasmas [25, 26]. Moreover, the presence of super-thermal electrons has been shown to modify the conditions for modulational instability, including its threshold and growth rate, in magnetized plasmas [27].

Studies on parametric interactions (PI) in acousto-optical semiconductors have shown notable enhancement in both dispersion and gain profiles in the presence of hot carriers [24]. In polar semiconductors, energetic electrons predominantly transfer their energy to the lattice through the emission of longitudinal optical (LO) phonons [28]. Additionally, the threshold conditions and operational behavior of singly resonant parametric oscillators in magnetized plasmas have been examined through analytical approaches [29].

In most earlier studies, the influence of carrier heating on the parametric interaction between electrons and LO phonons has been largely overlooked. The role of conduction band nonparabolicity (NPE) in affecting nonlinear behavior and amplification characteristics through hot carriers, analyzed via a semiclassical approach, remains insufficiently explored.

Therefore, the fundamental process of polaron-induced parametric interaction (PIPI) is considered here as a starting point to investigate the nonlinearity arising from energy-dependent effective electron mass (EEM) in a nonparabolic conduction band and the associated modifications in electron collision frequency (ECF).

Therefore, an analytical investigation of the threshold conditions and amplification behavior, based on the second-order susceptibility of a semiconductor plasma under the influence of a transverse magnetic field, is highly valuable. In this work, we explore how external factors such as the magnetic field strength, carrier density, and wave vector can be used to analytically determine the effect of carrier heating on this interaction. The structure of the paper is as follows: Section 2 presents the theoretical framework for evaluating the threshold and amplification characteristics of the nonlinear medium. Section 3 discusses the analytical findings along with graphical illustrations, and Section 4 summarizes the key conclusions.

2. Theoretical formulation

Any physical system undergoing oscillations shows nonlinear behavior when driven beyond a certain limit. In optical systems, such nonlinearity emerges under sufficiently strong illumination. This manifests in the polarization of the material, which then contains both linear and nonlinear components. The fundamental mechanism behind parametric processes is associated with the second-order optical susceptibility ($\chi^{(2)}$) in a nonlinear crystal, derived from the solution of Maxwell's nonlinear wave equation. In semiconductors, the high mobility of charge carriers makes carrier heating effects noticeable even at relatively low fields, giving rise to distinct nonlinear behavior [30]. Additionally, the conduction band's nonparabolicity introduces intrinsic nonlinearity through the energy-dependent effective mass (EEM). Carrier heating alters the electron collision frequency (ECF), while nonparabolicity modifies the EEM. The objective here is to quantify the individual contributions of these effects to the overall nonlinearity, providing a clearer understanding of hot carrier dynamics.

In this section, we examine the parametric amplification of the polaron mode resulting from three-wave interactions in a polar semiconductor subjected to irradiation by a relatively high-power laser, whose photon energy is well below the crystal's bandgap. The analysis is carried out under the following assumptions:

(i) The analysis employs the widely used hydrodynamic model of a homogeneous semiconductor plasma, which satisfies the condition $kl \ll 1$ (where k is the wave number and l is the electron mean free path). Within the hydrodynamic approximation [31], the charge carriers in the plasma are treated as a continuous, conducting fluid embedded in the crystalline lattice. This approach establishes a particle velocity distribution and allows the replacement of individual streaming electrons with a fluid representation, simplifying the analysis while retaining essential physical features. The model is characterized by key parameters such as the mean electron density (represented via the plasma frequency), mean drift velocity, and mean pressure (related to the collision frequency).

(ii) It is assumed that the polar semiconductor medium is illuminated by a spatially uniform ($|k_0| \approx 0$) pump electric field $\vec{E}_0 = \hat{x}E_0 \exp(-i\omega_0 t)$ while being subjected to a transverse DC magnetic field $\vec{B}_0 = \hat{z}B_0$.

(iii) The system is assumed to satisfy the phase-matching conditions, denoted as: $\omega_0 \approx \omega_1 + \omega_{pl}$ and $|\vec{k}_1| \approx |\vec{k}_{pl}| \approx k$ (say).

(iv) The parametric interaction of the pump field produces a polaron wave $(\omega_{pl}, \vec{k}_{pl})$ and a scattered signal wave (SW) $(\omega_1, \vec{k}_1)$, which are supported by the lattice vibrations and the electron plasma of the medium, respectively.

2.1 Nonlinearity due to EEM

The energy–momentum relationship $(\xi - k)$ for an electron in the conduction band of an n-type InSb crystal is expressed as [32]:

$$\xi(k) = \frac{\hbar^2 k^2}{2m_0} - \frac{\varepsilon_g}{2} + \frac{1}{2}\left(\varepsilon_g^2 + \frac{8}{3}p^2k^2\right)^{1/2}. \quad (1)$$

Here, ξ and $\hbar k$ represent the energy and momentum of an electron in the conduction band, m_0 is the free electron mass, ε_g is the energy band gap, and $p(\approx 8.5\times10^{-8}\,\text{eV})$ is a relevant matrix element [33]. From the energy dispersion relation in n-InSb (Eq. 1), it is evident that ξ is not strictly proportional to k^2, which highlights the nonparabolic nature of the conduction band. Although the motion of electrons in the periodic potential of a crystal is fundamentally quantum mechanical, one can approximate the dynamics classically by considering average quantum values of physical quantities. This allows the introduction of an energy-dependent effective mass **(**EEM**)** [31, 34], effectively reducing the quantum problem to a classical framework:

$$\frac{1}{m^*} = \left(\frac{1}{\hbar^2 k}\frac{d\xi}{dk}\right). \quad (2)$$

Using Eq. (1) in Eq. (2), the electron effective mass is considered to be energy-dependent, particularly near the bottom of the conduction band ($|\vec{k}| \to 0$), under the approximation $m^* \ll m_0$, where

$$m^* = \frac{A + \frac{\varepsilon_g}{k_B T_0}}{L}. \quad (3)$$

Here, A represents a ratio $\frac{2\langle\xi\rangle}{k_B T}$, which is of the order of (T_e/T_0) under Maxwellian distribution [34]. Here, $L = \frac{4p^2}{3\hbar^2 k_B T_0}$; k_B is the Boltzmann constant and T_0 is the lattice temperature.

When a semiconductor is subjected to a progressively stronger electric field, the carrier drift velocities eventually approach their saturation limit. Beyond this point, any further increase in the field primarily enhances the random thermal motion of the carriers, thereby increasing their average kinetic energy. Since kinetic energy is directly related to temperature, the electrons become "hot," meaning their effective

temperature exceeds the lattice temperature. After the steady state is reached, the applied field primarily increases the random thermal velocity of the carriers, and this can be taken as the main cause of carrier heating. The energy dependence of the electron effective mass, as expressed in Eq. (3), is therefore a significant source of nonlinearity in InSb [35].

2.2 Nonlinearity due to ECF

In general, when a high-intensity pump field interacts with a high-mobility n-type semiconductor, the electrons absorb energy and momentum from the field, causing their effective temperature (T_e) to rise above the lattice temperature (T_0). This increase in electron temperature reflects the phenomenon of carrier heating, which significantly affects the electronic and optical properties of the semiconductor.

This increase in electron temperature alters the momentum-transfer collision frequency of the electrons, which is primarily assumed to arise from acoustic phonon scattering. The modified collision frequency can be expressed as [30]:

$$\Gamma_e = \Gamma_{e0}\left(\frac{T_e}{T_0}\right)^{1/2}. \tag{4}$$

Here, T_e represents the effective electron temperature, and Γ_{e0} is the electron collision frequency at $T_e = T_0$. The steady-state electron temperature T_e can be obtained from the following energy balance equation:

$$\frac{\partial}{\partial t}\langle \xi \rangle = eE.v - \left\langle \frac{\partial \xi}{\partial t} \right\rangle_{coll}. \tag{5}$$

Here, v denotes the first-order perturbed electron velocity. The x- and y-components of this first-order electron fluid velocity can be expressed as:

$$v_{1x} = \frac{2\Gamma_{pl}}{4\Gamma_{pl}^2 + \omega_c^2}\left[-\frac{e}{m_e}E_{1x} - ik_1\left(\frac{k_B T}{m_e n_0}\right)n_1\right] \tag{6a}$$

and

$$v_{1y} = \frac{\omega_c}{4\Gamma_{pl}^2 + \omega_c^2}\left[-\frac{e}{m_e}E_{1x} - ik_1\left(\frac{k_B T}{m_e n_0}\right)n_1\right]. \tag{6b}$$

In this expression, $\Gamma_{pl} = \Gamma_e + \Gamma_{ph}$ represents the optical phonon decay constant, n_0 and n_1 denote the unperturbed and perturbed electron densities, respectively, and E_{1x} is the x-component of the first-order perturbed electric field.

$\left\langle \frac{\partial \xi}{\partial t} \right\rangle_{coll}$ represents the rate of energy loss per electron due to polar optical phonon (POP) scattering in an n-type III–V semiconductor. Under steady-state conditions, the power absorbed by each electron from the pump equals the power dissipated through POP scattering. Therefore, for moderate carrier heating, the electron temperature T_e can be expressed as:

$$\frac{T_e}{T_0} = 1 + \frac{e^2\Gamma_e}{2m_e}\frac{\tau(\omega_c^2 + \omega_0^2)}{[(\omega_c^2 + \omega_0^2)^2 + 4\Gamma_e^2\omega_0^2]}E_0.E_0^*, \tag{7}$$

where

$$\tau^{-1} = \left(\frac{2k_B\theta_D}{m_e\pi}\right)^{1/2} eE_{po}x_0.K_0\left(\frac{x_0}{2}\right).\frac{x_0^{1/2}\exp(x_0/2)}{\exp(x_0)-1};$$

$$E_{po} = \frac{m_e\hbar\omega_L}{\hbar^2}\left(\frac{1}{\varepsilon_\infty} - \frac{1}{\varepsilon_1}\right) \text{ (POP scattering potential);}$$

$$x_0 = \left(\frac{\hbar\omega_L}{k_B T_0}\right);\ K_0\left(\frac{x_0}{2}\right) \text{ (zeroth-order Bessel function);}$$

$\omega_c\left(=\frac{eB_0}{m_e}\right)$ is the cyclotron frequency,

θ_D is the Debye temperature of the medium,

ε_1 and ε_∞ are static and high-frequency dielectric permittivities of the medium, ω_L being the LO mode frequency. e and m_e are the charge and effective mass of electron, respectively.

2.3 Second-order nonlinear optical susceptibility

Since numerous semiconductor properties depend on the carrier velocity distribution [30], high-field-induced changes are likely to alter the medium's optical nonlinearities. The interaction between collective cyclotron excitations and longitudinal optical (LO) phonons generates an induced polarization in the medium. By employing the fundamental equations [29], applying the rotating wave approximation (RWA), and following the method adopted in Ref. [24], the induced polarization can be expressed as:

$$P^{(2)}(\omega_1) = \varepsilon_0\chi^{(2)}E_0E_{pl}^*. \tag{8}$$

Here, E_{pl} represents the space-charge field, and * denotes the complex conjugate of the quantity. Using Eq. (8), the second-order nonlinear susceptibility, $\chi^{(2)}$, can be expressed as:

$$\chi^{(2)} = \frac{-ike(NM)^{1/2}}{m_e\varepsilon_0\omega_{pl}}\left(\frac{\omega_0\omega_p^2}{\omega_0^2 - \omega_c^2}\right)\frac{QA_1T}{F_1}G^*. \tag{9}$$

Here we have neglected the Doppler shift under the assumption $\omega_0 >> \Gamma_{e0} > \vec{k}_0.\vec{v}_0$ and $N(=a^{-3})$ are the reduced mass of the di-atomic molecule and the number of unit cells per unit volume, respectively and a is the lattice constant of the crystal. ε_0 is dielectric permittivity of free space. ω_{pl} is the plasma frequency; ε is the dielectric permittivity of medium.

$$G = \left[\delta_2^2 - 2i\Gamma_{pl}\omega_{pl} - \frac{k^2A_2^2\left|\bar{E}\right|^2}{\delta_1^2 + 2i\Gamma_e\omega_1}\right]^{-1},$$

$$\delta_1^2 = A_1\bar{\omega}_p^2 - \omega_1^2,\ \delta_2^2 = A_1\bar{\omega}_p^2 - \omega_{pl}^2,$$

$$A_2 = \frac{\omega_0^2}{\omega_0^2 - \omega_p^2 - \omega_c^2},\ \bar{E} = \frac{(-e)E_{eff}}{m_e},\ A_1 = \frac{\omega_1^2}{\omega_1^2 - \omega_p^2 - \omega_c^2},$$

$$\bar{\omega}_p^2 = \left[\omega_p^2 + k_1^2\left(\frac{k_B T_e}{m^*}\right)\right]\left(\frac{4\Gamma_{pl}^2}{4\Gamma_{pl}^2 + \omega_c^2}\right),\ Q = X_1 + Y_1,$$

$$X_1 = \frac{4\Gamma_{pl}^2}{4\Gamma_{pl}^2 + \omega_c^2},\ Y_1 = \frac{\omega_{cpl}^2}{4\Gamma_{pl}^2 + \omega_{cpl}^2},\ \omega_{cpl} = \left(\frac{-e}{m_e} + \frac{q}{M}\right)B_0,$$

$$T = \frac{n_0 eq}{M} + \frac{Neq}{M} - \frac{n_0 e^2}{m_e} - \frac{Nq^2}{M},$$

$$q = \omega_L\left[\frac{M}{N}\varepsilon_0\left(\frac{1}{\varepsilon_\infty} - \frac{1}{\varepsilon_1}\right)\right]^{1/2}$$ (Callen effective charge) [36]

$$F_1 = \omega_{0,pl}^2 - \omega_{pl}^2 - 2i\Gamma_{pl}\omega_{pl};$$

$2\omega_{0,pl}^2 = \omega_p^2 + \omega_c^2 + \omega_L^2 + \left[(\omega_p^2 + \omega_c^2 + \omega_L^2)^2 - 4(\omega_p^2\omega_T^2 + \omega_c^2\omega_L^2)\right]^{1/2}$ is the frequencies of the normal modes in presence of magnetic field with $(k_0 \approx 0)$ and $(k_0 \perp B)$, arising from the coupling of the collective cyclotron excitations with the LO phonons via the macroscopic longitudinal electric field [37]. ω_T is the transverse optical phonon frequency. The above formulation reveals that the crystal susceptibility is influenced by the wave vector $\vec{k}$, carrier concentration n_0 and the transverse dc magnetic field through ω_c.

2.4 Threshold and amplification characteristics

The threshold pump amplitude, $[E_{0th}]_{para}$, which corresponds to the minimum pump field required to initiate polaron-induced parametric interaction (PIPI), can be determined as:

$$[E_{0th}]_{para} = \frac{m_e}{ekA_2}\left(1 - \frac{\omega_c^2}{\omega_0^2}\right)\delta_1\delta_2. \quad (10)$$

Parametric amplification occurs when the pump field exceeds this threshold value, and under suitable conditions, the corresponding gain can be expressed as:

$$\alpha_{para} = \frac{-k}{2\varepsilon_1}[\chi^{(2)}]_i E_0. \quad (11)$$

Here, α_{para} represents the nonlinear absorption coefficient. Equation (11) is thus used to analyze the amplification behavior of the scattered wave in the parametric process. The nonlinear parametric gain for both the signal and idler waves becomes feasible only when α\alphaα (from Eq. (9)) is positive, which occurs for pump electric fields satisfying $|E_0| > |[E_{0th}]_{para}|$.

3. Results and discussion

Using the theoretical approach outlined in Sect. 2, we have examined how nonparabolicity effects (NPE) influence the threshold conditions necessary for initiating parametric interactions and the resulting parametric amplification, where power is transferred from the pump wave to the signal wave in a III–V polar semiconductor. Numerical calculations were performed for an n-InSb sample subjected to a pulsed 10.6 μm CO_2 laser. The relevant physical parameters are taken from references [24, 29], and the analytical results are presented in Figs. 1–6.

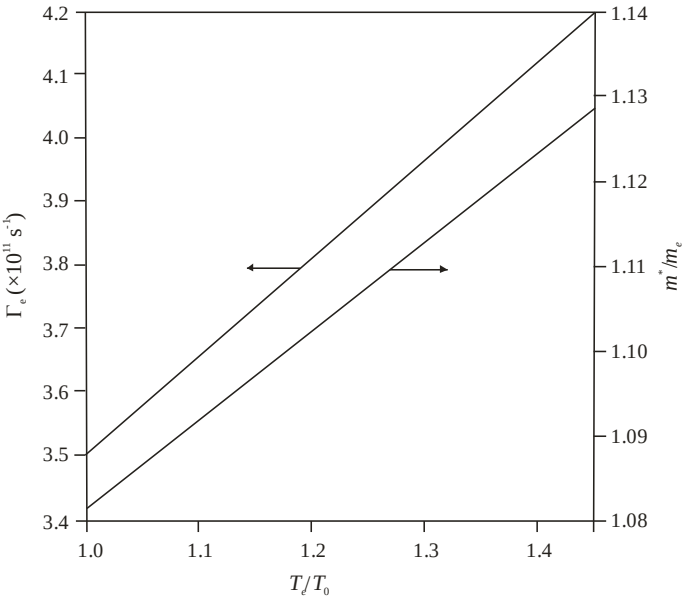

Figure 1: Variation of electron collision frequency (ECF, Γ_e) and normalized energy-dependent effective mass (EEM, m^*/m_e) as a function of the electron-to-lattice temperature ratio (T_e/T_0) at ω_c = 1.758×10^{12} s^{-1}.

Figure 1 illustrates the heating of carriers by the pump field (Eq. 7) along with the pump-induced variations of the normalized energy-dependent effective mass (EEM, Eq. 3) and electron collision frequency (ECF, Eq. 4). The plots indicate that both the ECF and normalized EEM increase approximately linearly with the electron-to-lattice temperature ratio. For example, at $T_e/T_0 = 1.4$, the normalized mass m^*/m_e reaches 1.1. This highlights the significance of carrier heating (CH) effects and NPE during interactions between an intense pump and a high-mobility semiconductor. Equation (7) also shows that a static transverse magnetic field can influence carrier heating in the range $\omega_c > \omega_0$. However, at very strong magnetic fields, cyclotron resonance effects become significant, making the present model inapplicable. Therefore, within the permissible range $\omega_c \le \omega_0$, the effect of the magnetic field on carrier heating is considered negligible.

3.1 Threshold characteristics

Using the given material parameters, we analyzed the threshold characteristics of the parametric interaction process. Equation (10) demonstrates that the threshold for parametric amplification strongly depends on the external magnetic field and the carrier concentration of the semiconductor. Figure 2 shows the variation of the threshold pump field $[E_{0th}]_{para}$ as a function of cyclotron frequency.

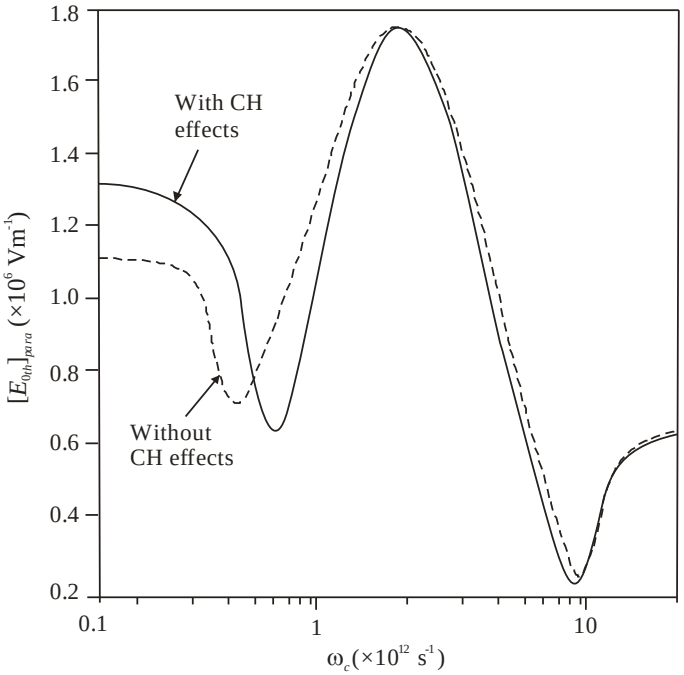

Figure 2: Threshold pump field ($[E_{0th}]_{para}$) as a function of cyclotron frequency (ω_c) for carrier density $n_0 = 4.2\times10^{23}$ m^{-3} and wave vector $k = 3\times10^8$ m^{-1}.

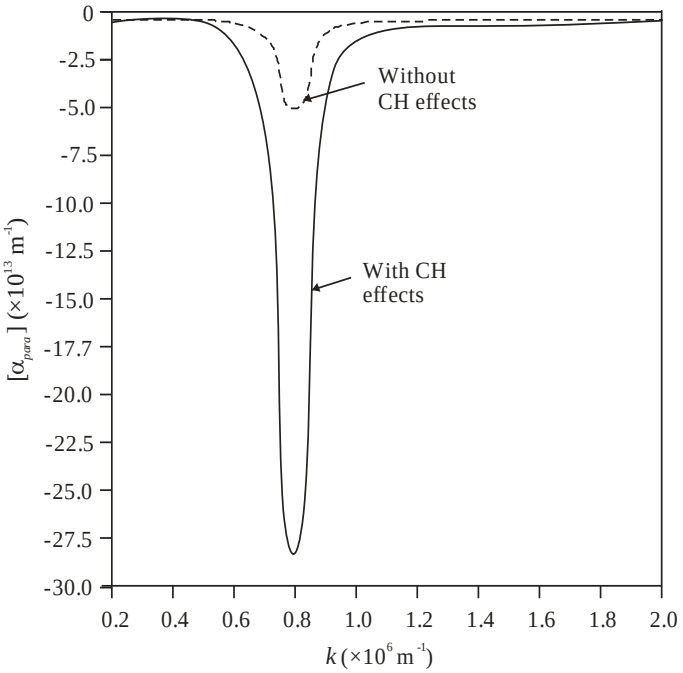

Figure 3: Dependence of the absorption coefficient (α_{para}) on wave vector k for $n_0 = 4.2\times10^{23}$ m^{-3} and $\omega_c = 1.758\times10^{12}$ s^{-1}.

The solid and dashed curves represent the threshold behavior with and without carrier heating (CH) effects, respectively. While both curves exhibit qualitatively similar trends, the comparison clearly highlights the significant role of CH effects in determining the onset of polaron-induced parametric interaction (PIPI).

Resonance between the cyclotron frequency and the signal frequency lowers the threshold pump field to its minimum in both scenarios. The presence of hot carriers shifts this minimum toward a higher magnetic field, which can be interpreted as a cooling effect of the magnetic field, consistent with earlier studies [38, 39]. Beyond the resonance frequency, increasing the magnetic field raises the threshold pump, reaching a peak. This increase is attributed to the reduction in $A_1\bar{\omega}_p^2$ in δ_1 term. At higher magnetic fields, the influence of carrier heating on threshold becomes negligible. The threshold pump reaches a minimum at a magnetic field corresponding to resonance between the cyclotron frequency and the polaron wave frequency in both cases. Therefore, the minimum threshold pump can be achieved at two distinct magnetostatic field values due to these two different resonance conditions:

$$\omega_c^2 = \omega_1^2\left(1-\frac{\bar{\omega}_p^2}{\omega_1^2}\right)-\omega_p^2 \text{ and } \omega_c^2 = \omega_{pl}^2\left(1-\frac{\bar{\omega}_p^2}{\omega_1^2}\right)-\omega_p^2 .$$

3.2 Parametric amplification characteristics

One of the main goals of the present study is to examine the parametric amplification arising from the imaginary part of the second-order optical susceptibility, $[\chi^{(2)}]_i$, as presented in Figs. 3–6. For significant parametric amplification, the pump field must exceed the threshold value ($|E_0| >> |[E_{0th}]_{para}|$). It is well established that a positive α_{para} corresponds to parametric absorption, whereas a negative α_{para} indicates parametric gain or amplification. In the figures, solid and dashed curves denote results with and without carrier heating (CH) effects, respectively.

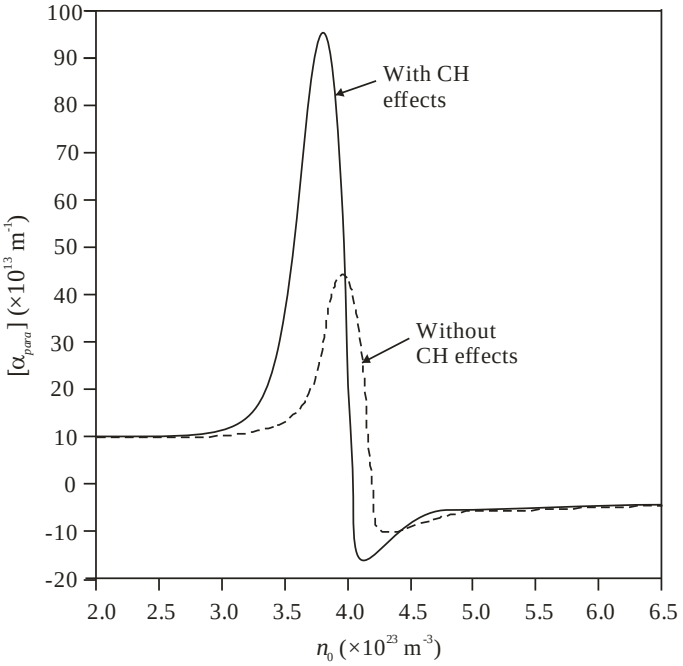

Figure 4: Variation of absorption coefficient (α_{para}) with carrier density n_0 at pump field $E_0 = 8\times10^6$ Vm^{-1}, wave vector $k = 3\times10^8$ m^{-1}, and $\omega_c = 1.758\times10^{12}$ s^{-1}.

Figure 3 illustrates the variation of the absorption coefficient α_{para} with the wave vector k. It is observed that at

$$k \approx \frac{\sqrt{(\delta_2^2 - 2i\Gamma_{pl}\omega_{pl})(\delta_1^2 - 2i\Gamma_e\omega_1)}}{A_2|\bar{E}|},$$

the absorption coefficient α_{para} shows strong gain, rapidly reaching its maximum value. Away from this resonance, α_{para} remains nearly constant with respect to k. Notably, the gain remains on the order of 10^{10} throughout the wave vector range considered.

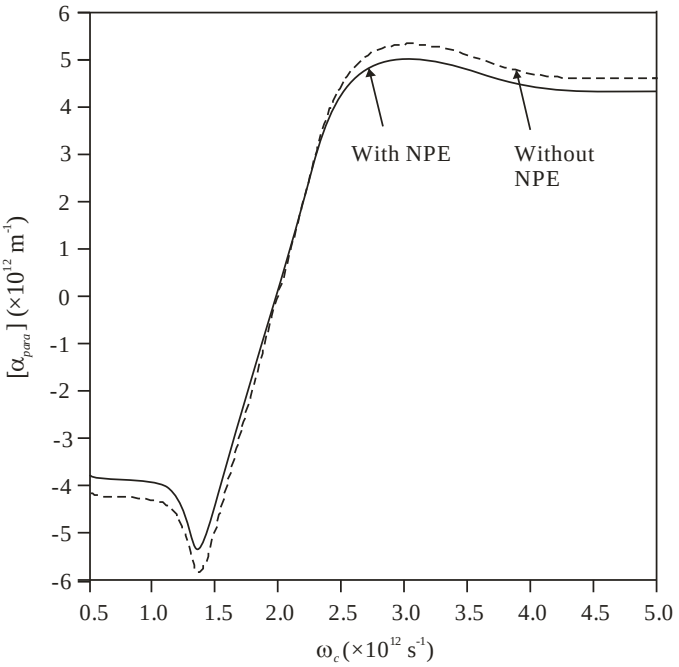

Figure 5: Absorption coefficient (α_{para}) as a function of cyclotron frequency (ω_c) for carrier density $n_0 = 4.2\times10^{23}$ m^{-3} and wave vector $k = 3\times10^8$ m^{-1}.

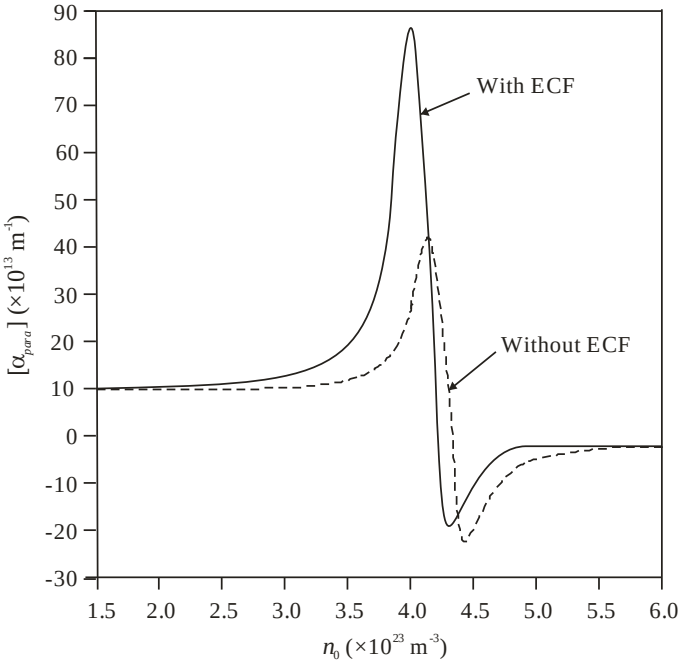

Figure 6: Variation of absorption coefficient (α_{para}) with carrier density n_0 at pump field $E_0 = 8\times10^6$ Vm^{-1}, wave vector $k = 3\times10^8$ m^{-1}, and $\omega_c = 1.758\times10^{12}$ s^{-1}.

Figure 4 depicts the variation of the absorption coefficient α_{para} with carrier density n_0, considering both cases with and without carrier heating (CH) effects. The analysis indicates that the most favorable carrier concentration range for parametric amplification lies between 3×10^{23} m^{-3} < n_0 <5×10^{23} m^{-3}, as CH effects significantly alter the electron collision frequency in this regime. At $n_0 = 4.1\times10^{23}$ m^{-3}, resonance between the polaron ($\omega_{0,pl}$) and signal (ω_l) frequencies produces maximum absorption, followed by a decrease in α_{para}, while resonance between the polaron cyclotron frequency and collective cyclotron excitation frequency leads to the highest parametric gain. Parametric amplification remains possible beyond $n_0 = 4.2\times10^{23}$ m^{-3} in both scenarios. Carrier heating causes the peak amplification to shift toward lower carrier densities because the rise in electron temperature increases the energy-dependent effective mass (EEM) and thermal energy, resulting in the observed shift compared to the case without CH effects.

Figure 5 illustrates the variation of the absorption coefficient α_{para} as a function of cyclotron frequency, considering both cases with and without the energy-dependent effective mass (NPE). At a wave vector of $k = 3\times10^8$ m^{-1}, α_{para} can take both positive and negative values. Parametric gain is observed only at lower magnetic fields, while beyond 0.2 T ($\omega_c = 2.512\times10^{12}$ s^{-1}), parametric absorption dominates due to resonance between the polaron cyclotron frequency and the collective cyclotron excitation frequency. The solid curve accounts for NPE by using the energy-dependent effective mass m^*, whereas the dashed curve uses the constant electron mass m_e in Eq. (9). As Eq. (9) shows an inverse relationship between susceptibility and electron mass, the inclusion of NPE (m^*/m_e = 1.08 at $\omega_c = 1.758\times10^{12}$ s^{-1}) increases the effective mass, which consequently reduces the parametric gain.

Figure 6 highlights the relative contributions of carrier heating (through modification of collision frequency, solid curve) and energy-dependent effective mass (EEM, dashed curve) to the nonlinear effects in homogeneous semiconductors in the infrared region. The analysis shows that nonlinearity arising from the modified collision frequency is weaker compared to the intrinsic nonlinearity due to EEM. The presence of EEM not only enhances the overall parametric gain but also shifts the peak gain toward higher carrier concentrations. For instance, a small increase of 0.2×10^{23} m^{-3} in carrier density leads to a 2% rise in parametric gain attributed to EEM. This sensitivity of gain to carrier concentration can be exploited for designing optical switching devices.

4. Conclusions

We have developed a theoretical framework based on the hydrodynamic model and coupled-mode theory to investigate polaron-induced parametric interactions (PIPI) in compound semiconductors. To analyze the effects of band nonparabolicity and carrier heating, we determined the modified second-order nonlinearity arising from the energy-dependent effective mass (EEM) and electron collision frequency (ECF). Using this approach, we calculated the second-order susceptibility and the threshold pump required to initiate PIPI. For practical applicability in fields such as ultrafast optical switches, electro-optic modulators, and infrared diagnostics, numerical estimations were performed for a well-studied compound semiconductor, indium antimonide (InSb).

It is found that the dominant contribution to nonlinearity arises from the energy-dependent effective mass (EEM). Both EEM and electron collision frequency (ECF) nonlinearity significantly modify the threshold and amplification characteristics. Nonparabolicity (NPE) and carrier heating (CH) effects are observed to enhance the parametric gain effectively. Additionally, the magnetic field acts as a control parameter, reducing the threshold pump field and further increasing parametric gain. However, beyond 0.2 T, CH effects become negligible. The combined inclusion of polaronic

effects and NPE is additive, resulting in a parametric gain enhancement on the order of 10^6 m^{-1}, compared to the gain of acoustic waves in a collision-dominated semiconductor plasma [40]. Therefore, it can be concluded that the second-order nonlinearity is substantially modified by nonparabolicity and carrier heating effects at low magnetic fields and moderate carrier concentrations.

References

[1] S. Baskoutas, E. Paspalakis, A.F. Terzis, Electronic structure and nonlinear optical rectification in a quantum dot: effects of impurities and external electric field, *J. Phys. Condens. Matter* **19** (2007) 395024.

[2] C.J. Zhang, K.X. Guo, Polaron effects on the third-order nonlinear optical susceptibility in asymmetrical semi-parabolic quantum wells, *Phys. B* **383** (2006) 183-187.

[3] X.L. Yu, S.L. Ban, Cyclotron resonance of a polaron in a realistic heterojunction and its pressure effect, *Eur. Phys. J. B* **52** (2006) 483.

[4] M.L. McMillan, Transition temperature of strong-coupled superconductors, *Phys. Rev*. **167** (1968) 331.

[5] X. Wu, D. Li, W.H. Sun, F. Gau, Z.J. Zang, R.W. Peng, Coupling of terahertz surface plasmon polaritons in corrugated stacks of dielectric and semiconductor, PIERS Online **5** (2009) 101.

[6] U. Merkt, M. Horst, J.P. Kotthaus, Magnetopolarons in inversion layers on InSb, *Phys. Scr*. **T13** (1986) 272.

[7] L.I. Korovin, I.G. Lang, S.T. Pavlov, New polaron effect in magnetooptic phenomena in a quantum well, *JETP* **65** (1997) 532.

[8] M.S. Sodha, A. Kumar, V.K. Tripathi, P.K. Kaw, Hot carrier diffusion induced instabilities of electromagnetic waves in plasmas and semiconductors, *Opto-electronics* **5** (1973) 509-516.

[9] J.T. Devreese, *Polarons and Polar Semiconductors*, North-Holland, Amsterdam (1972).

[10] S.D. Sarma, B.A. Mason, Band nonparabolicity effects on weak-coupling polarons in compound semiconductors, *Phys. Rev. B* **31** (1985) 1177.

[11] S. Huant, K. Karrai, Polaron Landau levels in InSb: A study of the influence of band nonparabolicity, *Phys. Rev. B* **37** (1988) 6955.

[12] M. Yamaguchi, T. Inaoka, M. Hasegawa, Electronic excitations in a nonparabolic conduction band of an n-type narrow-gap semiconductor, *Phys. Rev. B* **65** (2002) 085207.

[13] S. Ernst, A.R. Goni, K. Syassen, M. Cardona, Plasmon Raman scattering and photoluminescence of heavily doped n-type InP near the Γ-X crossover, *Phys. Rev. B* **53** (1996) 1287.

[14] M.P. Hasselback, P.M. Enders, Electron-electron interactions in the nonparabolic conduction band of narrow-gap semiconductors, *Phys. Rev. B* **57** (1998) 9674.

[15] L. Artus, R. Cusco, J. Ibanez, N. Blanco, G. Gonzalez-Diaz, Raman scattering by LO phonon-plasmon coupled modes in n-type InP, *Phys. Rev. B* **60** (1999) 5456.

[16] C.J. Zhang, K.X. Guo, Polaron effects on the optical absorptions in asymmetrical semi-parabolic quantum wells, *Phys. E* **39** (2007) 103-108.

[17] K.X. Guo, C.Y. Chen, Polaron effects on the optical rectification in electric-field-biased parabolic quantum wells, *J. Phys. Condens. Matter* **7** (1995) 6583.

[18] F.M. Yu, H.B. Chen, L.P. Zhou, Polaron effects on the change of refractive index in asymmetrical quantum wells, *Chin. J. Phys.* **49** (2011) 629-638.

[19] M. Glicksman, M.C. Steele, High electric field effects in *n*-indium antimonide, *Phys. Rev*. **110** (1998) 1204.

[20] M. Glicksman, M.C. Steele, Plasma pinch effects in indium antimonide, *Phys. Rev. Lett*. **2** (1959) 461.

[21] A.C. Prior, Avalanche multiplication and electron mobility in indium antimonide at high electric fields, *J. Electron Control* **4** (1988) 165-169.

[22] S. Guha, S. Ghosh, Convective instability in n-InSb in the presence of crossed electric and magnetic fields, *Phys. Stat. Sol. (a)* **41** (1977) 249-254.

[23] Renu, Sanjay, M. Singh, Hot carrier effects on Brillouin amplification in $A^{III}B^{V}$ and $A^{II}B^{VI}$ semiconductors, *J. Mod. Opt*. **69** (2022) 298–308.

[24] Renu, Sanjay, M. Singh, Hot carrier effects on Brillouin gain coefficients of magnetoactive doped semiconductors, *J. Opt*. **51** (2022) 386–396.

[25] Gopal, B.S. Sharma, M. Singh, Laser induced carrier heating effects on real and imaginary parts of Raman susceptibility of weakly-polar semiconductor magneto-plasmas, *J. Optoelectron. Adv. Mater* **24** (2022) 584–593.

[26] Gopal, B.S. Sharma, M. Singh, Effects of carrier heating on Raman susceptibility of weakly-polar semiconductor magneto-plasmas, *Trends Sci*. **19** (2022) 1487.

[27] M. Mottaghizadeh, P. Eslami, Cylindrical and spherical ion-acoustic solitons in electron-positive ion-negative ion plasmas, *Indian J. Phys*. **86** (2012) 71-75.

[28] A.V. Evteev, V.M. Ievlev, A.T. Kosilov, et al. Relaxed atomic structure of the interphase boundary in a “hemispherical nanoparticle-crystal” heterogeneous system, *Phys. Solid State* **49** (2007) 785–790.

[29] M. Singh, A. Sangwan, Sanjay, M. Singh, Parametric oscillation of acoustical phonon mode in magnetized doped III–V semiconductors, *J. Opt*. **50** (2021) 209–222.

[30] E.M. Conwell, *High Field Transport in Semiconductors*, Academic press, New York (1969) p 159.

[31] J. Pozhela, *Plasma and Current Instabilities in Semiconductors*, Oxford, Pergamon (1981) p 4, 26.

[32] E.O. Kane, Band structure of indium antimonide, *J. Phys. Chem. Solids* **1** (1987) 249-261.

[33] H. Ehrenreich, Electron scattering in InSb, *J. Phys. Chem. Solids* **2** (1987) 131-149.

[34] K. Seeger, *Semiconductor Physics*, Spinger-Verlag, New York (1973) p 14, 60.

[35] M.S. Sodha, A.K. Ghatak, V.K. Tripathi, *Self-Focusing of Laser Beams in Dielectrics, Plasmas and semiconductors*, Tata McGraw-Hill, New Delhi (1974) p 55, 60.

[36] H.B. Callen, Electric Breakdown in Ionic Crystals, *Phys. Rev*. **76** (1949) 1394.

[37] R. Kaplan, E.D. Palik, R.F. Wallis, S. Iwasa, E. Burstein, Y. Sawada, Infrared absorption by coupled collective cyclotron excitation-longitudinal-optic phonon modes in InSb, *Phys. Rev. Lett*. **18** (1967) 159.

[38] S.J. Buchsbaum, A.G. Chynoweth, W.L. Feldmann, Microwave emission from indium antimonide, *Appl. Phys. Lett*. **6** (1965) 67-69.

[39] T. Musha, F. Lindvall, J. Hagglund, Microwave emission from InSb for low electric fields, *Appl. Phys. Lett*. **8** (1966) 157-159.

[40] M. Singh, P. Aghamkar, S.K. Bhakar, Parametric dispersion and amplification in semiconductor-plasmas, *Opt. Laser Technol*. **41** (2009) 64–69.